Biochimica et Biophysica Acta 1798 (2010) 114–121

Contents lists available at ScienceDirect

Biochimica et Biophysica Acta

journal homepage: www.elsevier.com/locate/bbamem

Structure, dynamics and mapping of membrane-binding residues of micelle-bound antimicrobial peptides by natural abundance ^{13}C NMR spectroscopy

Guangshun Wang *

Eppley Institute for Research in Cancer and Allied Diseases, University of Nebraska Medical Center, 986805 Nebraska Medical Center, Omaha, NE 68198-6805, USA

ARTICLE INFO

Article history:
Received 15 April 2009
Received in revised fom 8 June 2009
Accepted 30 July 2009
Available online 12 August 2009

Keywords:
Antimicrobial peptides
Chemical shifts
Dynamics
HSQC wave
Membrane-binding residues
Membrane proteins
Micelles
NMR waves

ABSTRACT

Worldwide bacterial resistance to traditional antibiotics has drawn much research attention to naturally occurring antimicrobial peptides (AMPs) owing to their potential as alternative antimicrobials. Structural studies of AMPs are essential for an in-depth understanding of their activity, mechanism of action, and in guiding peptide design. Two-dimensional solution proton NMR spectroscopy has been the major tool. In this article, we describe the applications of natural abundance ^{13}C NMR spectroscopy that provides complementary information to 2D ^{1}H NMR. The correlation of $^{13}C\alpha$ secondary shifts with both 3D structure and heteronuclear ^{15}N NOE values indicates that natural abundance carbon chemical shifts are useful probes for backbone structure and dynamics of membrane peptides. Using human LL-37-derived peptides (GF-17, KR-12, and RI-10), as well as amphibian antimicrobial and anticancer peptide aurein 1.2 and its analog LLAA, as models, we show that the cross peak intensity plots of 2D ^{1}H–$^{13}C\alpha$ HSQC spectra versus residue number present a wave-like pattern (HSQC wave) where key hydrophobic residues of micelle-bound peptides are located in the troughs with weaker intensities, probably due to fast exchange between the free and bound forms. In all the cases, the identification of aromatic phenylalanines as a key membrane-binding residue is consistent with previous intermolecular Phe-lipid NOE observations. Furthermore, mutation of one of the key hydrophobic residues of KR-12 to Ala significantly reduced the antibacterial activity of the peptide mutants. These results illustrate that natural abundance heteronuclear-correlated NMR spectroscopy can be utilized to probe backbone structure and dynamics, and perhaps to map key membrane-binding residues of peptides in complex with micelles. ^{1}H–$^{13}C\alpha$ HSQC wave, along with other NMR waves such as dipolar wave and chemical shift wave, offers novel insights into peptide–membrane interactions from different angles.

1. Introduction

In the Protein Data Bank, the number of structures of membrane proteins is far less than that of globular proteins. To a large extent this situation might be attributed to the difficulty in expression and purification of membrane proteins and their reconstitution into a proper detergent required for the formation of useful crystals for X-ray diffraction. High-resolution NMR spectroscopy provides an alternative approach for structural determination. This versatile technique enables the structural determination of membrane proteins in either liquid or solid state. For solution NMR studies, it is necessary to solubilize the protein in suitable detergents such as dodecylphosphocholine (DPC), lysolipids, or small bicelles [1]; for solid-state NMR, the proteins are usually reconstructed in lipid bilayers or large bicelles [2]. While structural studies of large receptors with multiple transmembrane helices are in progress [3,4], there is also high interest in structural studies of smaller membrane proteins such as amyloid peptides [53,54] and antimicrobial peptides (AMPs). The high interest in AMPs may be because of their potential to be developed into novel antimicrobials as alternatives to drug-resistant antibiotics [5–8]. In the updated antimicrobial peptide database (APD2, with more than 1400 peptide entries), ~90% of the peptides collected contain less than 45 residues [9,10]. Because membrane peptides are usually resistant to crystallization, NMR has been the dominating technique in structural elucidation of AMPs. The small size of AMPs made solid-phase synthesis an ideal method for peptide preparation. On one hand, solid-phase synthesis enables the incorporation of ^{2}H, ^{13}C, ^{19}F, and ^{15}N isotopes into peptide sites of interest for probing structure and dynamics by solid-state NMR methods [11–14,70,71]. On the other hand, synthetic peptides can also be directly utilized for 3D structural

Abbreviations: NMR, nuclear magnetic resonance; AMPs, antimicrobial peptides; APD2, the antimicrobial peptide database version 2; D8PG, dioctanoyl phosphatidylglycerol; DPC, dodecylphosphocholine; DQF-COSY, double-quantum filtered correlation spectroscopy; DSS, 2,2-dimethyl-silapentane-5-sulfonate sodium salt; HSQC, heteronuclear single-quantum coherence spectroscopy; LLAA, LL-37-derived aurein 1.2 analog; MIC, minimal inhibitory concentration; NOE, nuclear Overhauser effect; NOESY, nuclear Overhauser enhancement spectroscopy; PGs, phosphatidylglycerols; SDS, sodium dodecylsulfate; TOCSY, total correlation spectroscopy

* Eppley Institute, Room ECI3018, University of Nebraska Medical Center, 986805 Nebraska Medical Center, Omaha, NE 68198-6805, USA. Tel.: +1 402 559 4176; fax: +1 402 559 4651.
E-mail address: gwang@unmc.edu.

0005-2736/$ – see front matter © 2009 Elsevier B.V. All rights reserved.
doi:10.1016/j.bbamem.2009.07.028

determination by solution NMR [5–8]. Indeed, 95% of the structures collected in APD2 are solved by solution NMR in water or in organic solvents or detergent micelles as membrane-mimetic models [9].

Because the major anionic lipids in bacterial membranes are phosphatidylglycerols (PGs) [15], we have demonstrated the use of short-chain anionic PGs as a new membrane model for structural determination of membrane peptides by solution NMR spectroscopy [16–18]. The major findings have been summarized in our previous publications [6,19]. The unique spectral window presented in the dioctanoyl phosphatidylglycerol (D8PG) sample, but not in SDS nor DPC micelles, facilitates the observation of long-desired intermolecular Arg–PG NOE cross peaks by solution NMR for the first time [20–23].

The 3D structures of most of the micelle-bound AMPs were determined based primarily on NOE-derived distance restraints. Complementary angle restraints, usually derived from scalar coupling constants, are not readily measured due to broad spectral lines of micelle-bound peptides (10–15 Hz). An alternative approach to obtaining backbone angles is based on a set of heteronuclear chemical shifts. We previously demonstrated that ^{15}N and ^{13}C chemical shifts could be measured at natural abundance and inclusion of chemical shift-derived backbone angles led to improvement in the quality of distance-derived NMR structures [20].

There are yet other limitations with classic 2D ^{1}H NMR, which we intend to deal with in this study. For example, how can one obtain dynamic information for micelle-bound AMPs in the absence of isotope labeling? Using human LL-37 as a model, we show that secondary $^{13}C\alpha$ chemical shifts are correlated with ^{15}N NOE values. This observation provides an approach for probing peptide dynamics based on natural abundance ^{13}C chemical shifts. In addition, it is not trivial to define membrane-binding residues using the well-established chemical shift mapping method owing to a global conformational change of many AMPs from the free to bound states. We illustrate here that 2D ^{1}H–^{13}C HSQC spectra appear to contain information for micelle binding of AMPs. For this purpose, multiple LL-37-derived segments and aurein 1.2 are used as model peptides (sequences in Table 1). As the only cathelicidin in humans, the protective role of human LL-37 against infectious diseases is well established clinically as well as in animal models [24–26], and LL-37 is perhaps one of the best-studied AMPs [55–63] as reflected by an exponential growth in the related literature [39]. Aurein 1.2 is a 13-residue antimicrobial and anticancer peptide discovered in Australian bell frogs [27]. Both solution and solid-state NMR methods have been utilized to investigate its interactions with phospholipids [14,20,21].

2. Materials and methods

2.1. Materials

GF-17, KR-12 and its single-residue peptide mutants, RI-10, aurein 1.2, and LLAA (Table 1) with C-terminal amidation (>95% pure) were synthesized and purified by Genemed Synthesis (San Antonio, TX). Perdeuterated SDS (98% D) and deuterium oxide (99.9% D) were purchased from Cambridge Isotope Laboratories (Andover, MA). All chemicals were used without further purification.

Table 1
Primary structures of membrane peptides.

Peptide	Amino acid sequence
LL-37	LLGDFFRKSKEKIGKEFKRIVQRIKDFLRNLVPRTES
GF-17[a]	GFKRIVQRIKDFLRNLV-NH_2
KR-12	KRIVQRIKDFLR-NH_2
RI-10	RIVQRIKDFL-NH_2
Aurein 1.2	GLFDIIKKIAESF-NH_2
LLAA[b]	RLFDKIRQVIRKF-NH_2

[a] C-terminal amidation of this peptide, as well as others, is indicated by NH_2.
[b] LL-37-derived aurein 1.2 analog [21].

2.2. Antibacterial activity assays

The antibacterial activities of KR-12 and its single-residue mutants were determined using the standard broth microdilution method [20]. In brief, a 5 ml culture was grown overnight in Luria–Bertani (LB) medium. A fresh culture was inoculated with a small aliquot of the overnight culture and incubated at 37 °C (250 rpm) until the optical density reaches ~0.5. The culture was then diluted and 90 µl portioned into a 96-well microplate with ~10^6 CFU per well. A series of peptide solutions (10 µl) with two-fold dilution was added. The assays were performed in triplet for each peptide. The plate was incubated at 37 °C overnight (~16 h) and read on an Ultra Microplate Reader at 630 nm (Bio-TEK Instrument). The minimal inhibitory concentration (MIC) of a peptide is defined as the lowest peptide concentration that fully inhibits the bacterial growth.

2.3. NMR spectroscopy

The NMR samples were prepared by mixing the peptide with SDS-d_{25} at a molar ratio of 1:40 (2 mM peptide), containing 10% D_2O as the field-locking signal. Such a ratio was found to be sufficient to stabilize the structure of the peptide. The pH of each sample was adjusted by using microliter aliquots of HCl or NaOH solution and measured directly in the 5-mm NMR tube with a micro-pH electrode (Wilmad-Labglass).

NMR data were recorded on a Varian INOVA 600 MHz NMR spectrometer equipped with a triple-resonance cryoprobe with a *z*-axis gradient. A set of NMR spectra was collected for each peptide using States-TPPI. NOESY spectra [28] were acquired at a mixing time of 100 ms for peptide/micelle complexes. TOCSY experiments were performed with a mixing time of 75 ms using a clean MLEV-17 pulse sequence [29]. Typically, 2D homonuclear spectra were collected with 512 increments (16–32 scans each) in t1 and 2K data points in t2 time domains using a spectral width of 8510.6 Hz in both dimensions with the ^{1}H carrier on the water resonance. The water signal was suppressed by WATERGATE [30] in NOESY and TOCSY experiments. To obtain backbone $^{13}C\alpha$ chemical shifts, gradient-enhanced HSQC spectra [31] between ^{1}H and ^{13}C were collected at natural abundance. The ^{1}H and ^{13}C carriers were set at 4.77 and 36.37 ppm, respectively. Typically 80 increments (256 scans) were collected for the aliphatic ^{13}C (spectral width 12,000 Hz) dimension.

NMR data were processed on a Silicon Graphics Octane workstation (SGI) using the NMRPipe software [32]. For 2D homonuclear spectra such as NOESY, the time domain data were apodized by a 63° shifted squared sine-bell window function in both dimensions, zero-filled prior to Fourier transformation. For HSQC, the data in the indirect dimension was doubled by linear prediction prior to Fourier transformation. Since anionic DSS is known to interact with cationic peptides [16], proton chemical shifts of the peptides were referenced to external DSS at 0.00 ppm and ^{13}C and ^{15}N chemical shifts were referenced as described [20]. NMR data were analyzed with NMRDraw in the NMRPipe package [32] or PIPP [33].

3. Results

3.1. Correlation of 3D structure, dynamics, and secondary $^{13}C\alpha$ chemical shifts of micelle-bound LL-37

The 3D structure of human LL-37 in complex with detergent micelles has recently been determined [7,23]. In SDS micelles, the peptide adopts a long amphipathic helix from residues 2 to 31 with the remaining residues disordered (Fig. 1a). This structure corresponds nicely to the $^{15}N\{^{1}H\}$ NOE plot (Fig. 1b). The NOE plot indicates that only the C-terminal residues 33–37 are mobile on the ps–ns time

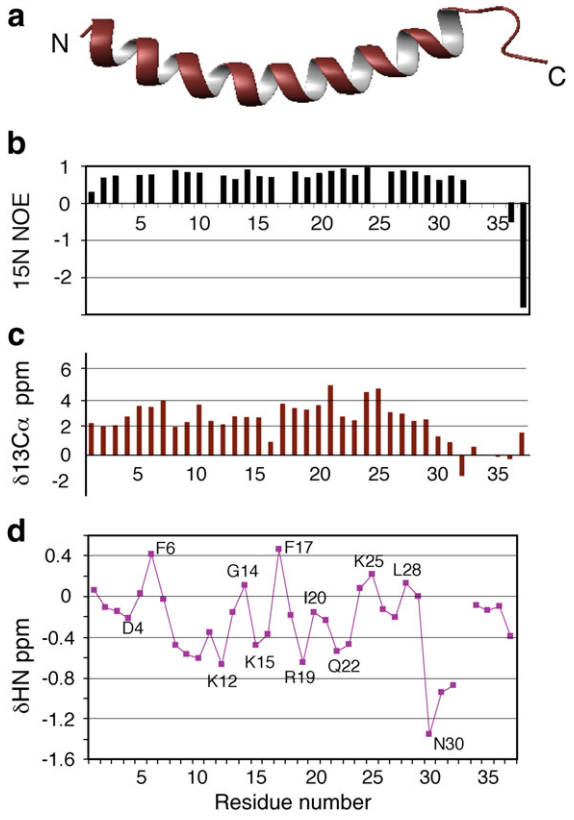

Fig. 1. Correlation of structure, dynamics, with ^{13}Cα secondary shifts. a, Ribbon diagram of human LL-37 in SDS micelles determined as described elsewhere [23]. b, Heteronuclear NOE plot of LL-37 in SDS recorded and calculated as described [23]. c, ^{13}Cα secondary shifts versus residue number. d, Secondary amide shifts of LL-37 in SDS. Secondary shifts are the chemical shift differences between the measured and the random values in ref. [38]. See the text for further details.

scale. Fig. 1c displays the ^{13}Cα secondary shifts (δ^{13}Cα) of LL-37, i.e. the chemical shift differences between the measured and the random coiled values [34]. It is evident that continued positive shifts for residues 2–31 correspond exactly to the helical region determined by 3D heteronuclear NMR using isotope-labeled peptide samples [23]. Furthermore, residues 32–37 showed small δ^{13}Cα deviations (Fig. 1c), consistent with the lack of a defined structure in that region (Fig. 1a). Thus, ^{13}Cα secondary shifts contain both structural and dynamic information. Because heteronuclear ^{15}N NOE values are not measured for synthetic peptides without isotope labeling, the correlation observed in Fig. 1 might be applied to probing peptide dynamics using natural abundance ^{13}Cα chemical shifts.

3.2. Natural abundance ^{13}Cα secondary shifts as a probe for peptide structure and dynamics

To illustrate the application of the correlation in Fig. 1, we collected 2D ^{1}H–^{13}C HSQC spectra for several peptides at natural abundance (Fig. 2). GF-17 (Table 1) was engineered based on one of the most active regions of human LL-37 identified by NMR [35]. It corresponds to residues 17–32 of LL-37 with an additional Gly at the N-terminus and an amide NH_2 at the C-terminus of the peptide to improve stability. In the following description, the residue numbering as in LL-37 is maintained in GF-17 and its shorter segments in Table 1. GF-17 showed strong activities against both Gram-positive and Gram-negative bacteria [72]. It also showed an inhibitory effect on HIV [37] and could kill cancer cells as well [35]. The natural abundance HSQC spectrum of GF-17 bound to SDS micelles (peptide/SDS ratio of 1:40) is provided in Fig. 2a. Remarkably, the ^{1}H–^{13}Cα cross peaks are well resolved. These cross peaks were assigned based on the known ^{1}H assignments achieved by using the standard NMR method [38]. Based on the ^{13}C chemical shifts of GF-17, we calculated ^{13}Cα secondary shifts and plotted in Fig. 3a. Since the ^{13}Cα secondary shifts for residues 17–31 of GF-17 are greater than 1 ppm [36], they are predicted to be helical. These secondary shifts also suggest that this region of the peptide is rigid when bound to the SDS micelles. However, the C-terminal residue V32, with a small δ^{13}Cα less than 1 ppm, appears to be mobile.

KR-12 (Table 1) was identified as the smallest antibacterial peptide of LL-37 [23]. Its 3D structure was determined in D8PG micelles. Residues 20–28 are helical (Fig. 4a). To provide additional insight into peptide–micelle interactions, we also collected a set of NMR spectra for KR-12 in SDS micelles. Its ^{1}H–^{13}Cα HSQC spectrum is given in Fig. 2b. The cross peaks are well resolved, allowing complete assignments of all ^{1}H–^{13}Cα cross peaks at natural abundance. Compared to GF-17 (Fig. 2a), most of cross peaks of the residues of KR-12 appeared at similar spectral regions and only terminal residues K18, R19, and R29 showed significant shifts. Based on the ^{13}Cα secondary shift plot (Fig. 3b), residues 19–28 are predicted to be helical. Thus, the structures of KR-12 are similar in SDS and D8PG micelles. In these two micelles, similar structures were also observed for bacterial membrane anchor [16], aurein 1.2 [20], and FK-13 (the antibacterial core region of LL-37) [35]. Furthermore, the δ^{13}Cα deviations suggest that, except for R29, the entire peptide is rigid in complex with micelles.

To further understand peptide–micelle interactions, we also investigated an even shorter peptide RI-10, which was obtained by deleting both the N- and C-terminal residues of KR-12 (Table 1). The truncation of the two terminal cationic residues disrupted the antibacterial activity of the peptide against *Escherichia coli* K12 [23]. The 2D HSQC spectrum of this peptide in complex with SDS is presented in Fig. 2c. Again, the peaks are well resolved, allowing full signal assignments of the ^{1}H–^{13}Cα cross peaks. According to the ^{13}Cα secondary shift plot (Fig. 3c), residues 20–27 of RI-10 remain helical. Therefore, the loss of two cationic residues and a shortened amphipathic helix of RI-10 compared to KR-12 may be responsible for the loss of antimicrobial activity.

While the Australian group determined the structure in trifluoroethanol (TFE) [27], we previously determined the 3D structure of aurein 1.2 in complex with SDS micelles [20]. This short antimicrobial peptide is entirely helical in SDS micelles (Fig. 4b). Its ^{1}H–^{13}C HSQC spectrum is presented in Fig. 2d. To get insight into peptide backbone motion, we also calculated ^{13}Cα secondary shifts for aurein 1.2 (Fig. 3d). Residues 2–12 displayed positive secondary shifts greater than 1 ppm, consistent with an all-helical structure. The terminal F13 showed a smaller ^{13}Cα deviation and may be slightly more mobile than other residues.

3.3. ^{1}H–^{13}Cα cross peak intensity plots

Previously, we identified the core antimicrobial region of human LL-37 based on the peak intensity differences in 2D TOCSY spectra [35]. While micelle-bound residues displayed weak to no cross peak relays from backbone amide protons to side chains, non-micelle-bound or weakly binding residues showed strong TOCSY relays. A further examination of the TOCSY H^N-Hα cross peak intensity plots of LL-37-derived peptides in complex with micelles revealed a wave-like pattern. In this study, peak intensities are represented by peak heights. Although hydrophobic residues tend to have weaker intensities in several cases, no consensus was observed. We then examined the peak intensity plots of ^{1}H–^{13}C HSQC spectra of GF-17, KR-12, RI-10, aurein 1.2 and its analog LLAA bound to SDS micelles (Fig. 5). A wave-like pattern is evident in all the cases. We found that these wave patterns did not depend on the NMR programs used to measure peak intensities, since we observed similar results with NMRPipe [32] or PIPP [33] (not shown). We also obtained identical results using NMRPipe when the spectral threshold was set at different levels that determine the number of contours visible to human eyes. It is interesting to note that the residues at the troughs of the waves have lowest peak intensities and are usually hydrophobic. In the case of GF-17 (Fig. 5a), residues I20, V21, I24, F27, and L28 are

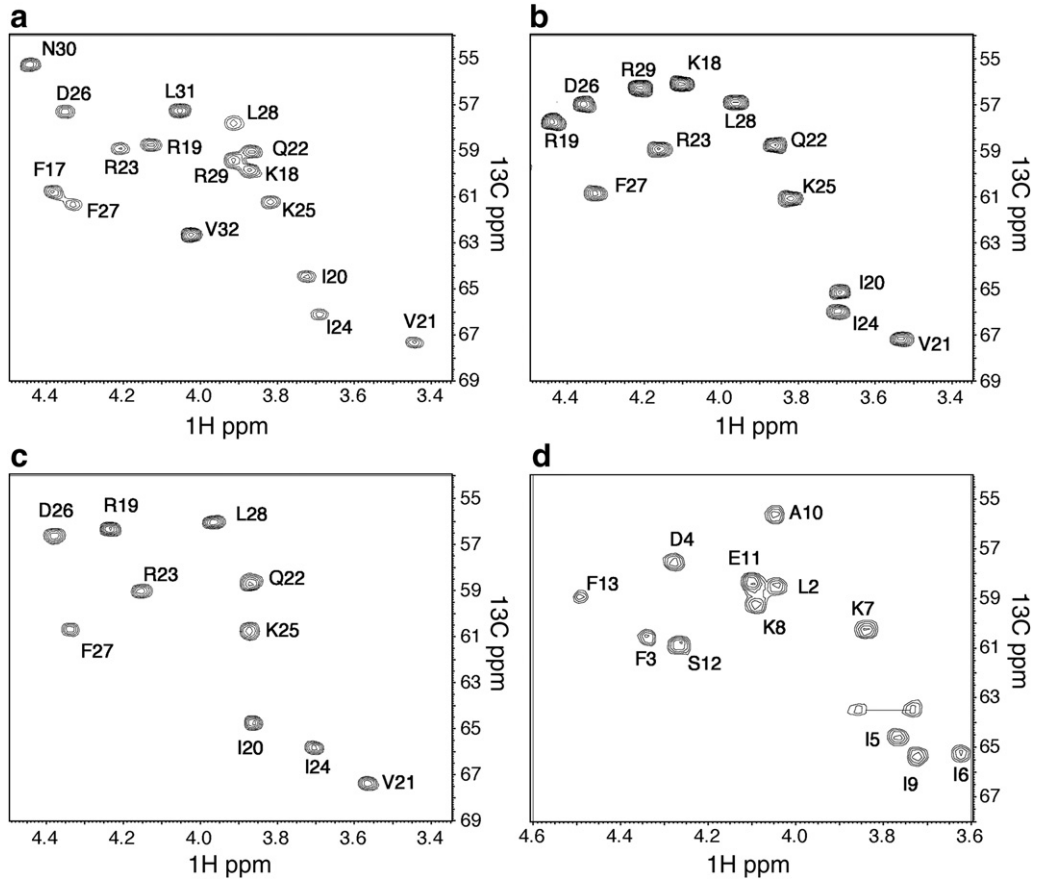

Fig. 2. Natural abundance $^{1}H–^{13}C\alpha$ HSQC spectra of GF-17 (a), KR-12 (b), RI-10 (c), and aurein 1.2 (d) in complex with SDS micelles. Spectra were collected at a peptide/SDS molar ratio of 1:40, pH 5.4 and 25 °C.

located in the troughs. The increase in peak intensity in the C-terminus may imply increased motions in that region of the polypeptide chain. Of outstanding interest is that this set of hydrophobic residues I20, V21, I24, F27, and L28 identified in the GF-17 plot consists of the hydrophobic surface of KR-12 (Fig. 4a bottom). Since KR-12 was identified as the smallest antimicrobial peptide from LL-37, those five hydrophobic residues of GF-17 with weaker intensities (Fig. 5a) are proposed to be essential membrane-binding residues. Indeed, when hydrophobic residue I20, or I24, or L28 of KR-12 was changed to Ala, the antimicrobial activities of the resulting three peptide mutants reduced significantly and were inactive against *E. coli* K12 till ~300 μM (see Methods). Under the same condition, the MIC of KR-12 itself was found to be ~20 μM.

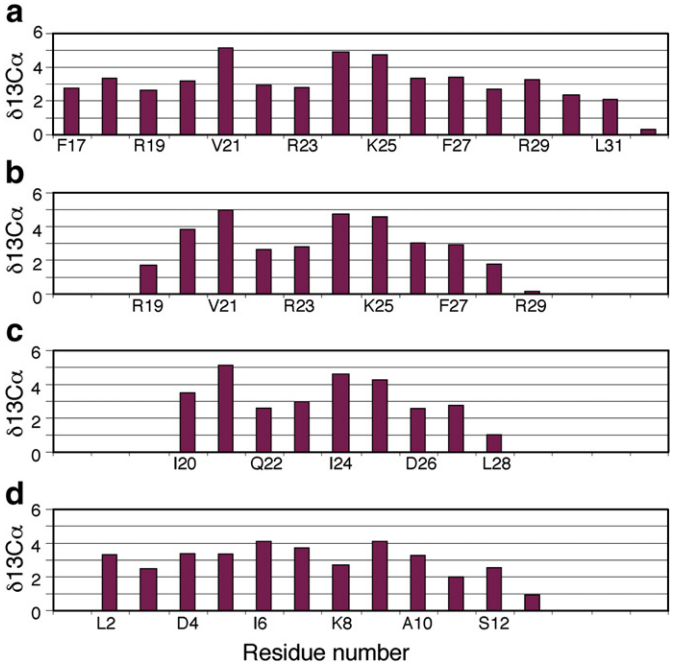

Fig. 3. $^{13}C\alpha$ secondary shifts of GF-17 (a), KR-12 (b), RI-10 (c), and aurein 1.2 (d) in complex with SDS micelles. Chemical shifts were obtained from Fig. 2.

In the HSQC peak intensity plot of KR-12 itself in SDS (Fig. 5b), four hydrophobic residues I20, V21, I24, and F27 recurred as trough residues. Compared to those in GF-17 (Fig. 5a), peak intensities for both residues L28 and R29 increased, presumably due to increased motions of the residues at the peptide termini. Indeed, these residues displayed smaller $^{13}C\alpha$ deviations (Fig. 3, cf. panels a and b).

For inactive peptide RI-10 in complex with SDS micelles, its HSQC peak intensity plot is displayed in Fig. 5c. Only three hydrophobic residues V21, I24, and F27 are trough residues. It is evident that the number of the trough residues (i.e. membrane-anchoring residues) from GF-17, KR-12, to RI-10 decreases with the shortening of the peptide length. Such a trend provides a good interpretation for reduced antimicrobial activity of these LL-37 peptides from GF-17 (MIC 10 μM), KR-12 (MIC 20 μM), to RI-10 (inactive) [23; this study], indicating the importance of these membrane-targeting residues for peptide activity.

As a different example, we also evaluated the peak intensity plot of aurein 1.2 in complex with SDS micelles (Fig. 5d). The residues that occupy the trough positions of the wave are F3, I6, A10, and F13, which are all hydrophobic. These residues aligned well on the hydrophobic face of the amphipathic structure of aurein 1.2 determined in detergent micelles (Fig. 4b). The identification of F13 as an essential anchoring residue in aurein 1.2 is consistent with its critical role in conferring

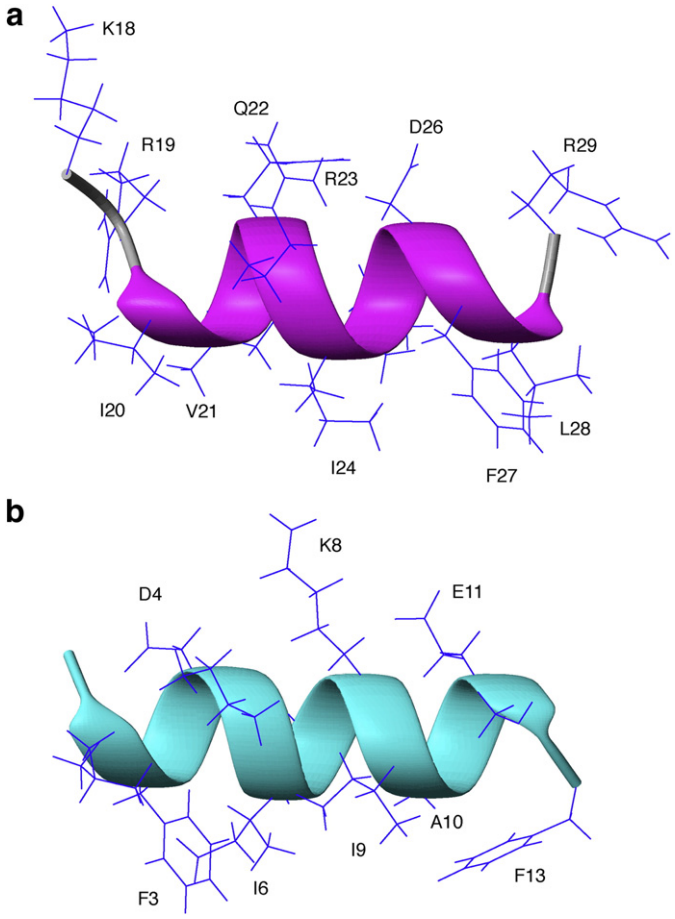

Fig. 4. 3D structures of KR-12 (a) in D8PG and aurein 1.2 (b) in SDS. The details for determination of these structures are provided in refs. [23] and [20], respectively. The figures were made by using MOLMOL [52].

activity to the peptide. We found that a change of F13 to either phenylglycine or W13 reduced peptide's activity [21]. A phenylglycine differs from a phenylalanine by only a β-CH_2 group. Structurally, the F13 aromatic ring in aurein 1.2 bends toward the side chains of residues I9 and A10 to form a local hydrophobic cluster (Fig. 4b). Shortening the F13 side chain appears to hinder the effective packing of hydrophobic side chains in this hydrophobic cluster, thereby reducing the membrane perturbation power of aurein 1.2. Using intermolecular NOE measurements, we observed that both F3 and F13 interact with D8PG [20], substantiating their role as membrane anchors.

Fig. 5e presents the HSQC wave of LLAA in SDS micelles [21]. LLAA was obtained by reversing the sequence of the antimicrobial core region (residues 17–29) of LL-37 (Table 1). The peptide remained antibacterial after sequence reversal. Residues F3, K5, I6, V9, I10, and F13 of LLAA are located in the troughs. Compared to aurein 1.2, additional residues K5 and V9 were identified as key binding residues. Since aromatic ring protons are well resolved, F3 and F13 served as excellent probes for us to detect peptide–lipid NOE cross peaks. These dipolar interactions indicate that both F3 and F13 are located in the head group region of D8PG and slightly penetrated into acyl chains [21]. Taken together, our results support that the identified hydrophobic surface of LLAA is in direct contact with lipid micelles.

The above examples comprise peptides in complex with SDS micelles. To evaluate the effect of micelle types, we also collected a set of NMR spectra for KR-12 in DPC micelles. The spectra were assigned based on 2D NMR techniques. No evidence was found for structural changes. The HSQC wave of KR-12 in DPC is shown in Fig. 5f. The wave pattern of the peptide in DPC clearly resembles that in SDS (Fig. 5b). In particular, the anchoring residues I20, V21, I24, and F27 are identical to those found in SDS micelles, indicating that this peptide uses the same set of hydrophobic residues to bind both types of micelles. Note that the wave pattern in Fig. 5f persisted upon increasing temperature from 25 to 45 °C (not shown). In the presence of SDS, R29 of KR-12 was implied to be mobile (Fig. 3b). The same residue may be even more mobile in DPC since the peak intensity of R29 doubled in Fig. 5f. The slightly increased motion of residue R29 of KR-12 in DPC may result from reduced interactions of this cationic residue with the zwitterionic head group of DPC compared to the anionic head group of SDS.

4. Discussion

Structural studies of membrane peptides in micelles are routinely carried out by classic 2D NMR techniques [38]. The short length of these peptides facilitates chemical synthesis for solution NMR studies, usually without recording ^{13}C and ^{15}N chemical shifts. It appears that obtaining isotope-labeled AMPs is not without difficulty. The toxicity of these peptides to the expression cells made it necessary to express them as fusion proteins. The aggregation of LL-37 might have caused the poor cleavage of fusion proteins by proteases. These problems may be the reason for low yields of recombinant LL-37 in the published bacterial expression systems (0.3–1.7 mg per liter) [57–59]. As a consequence, there is great interest in improving our understanding of AMP–membrane interactions by extracting ^{13}C and ^{15}N chemical shifts from natural abundance NMR spectroscopy of unlabeled peptides.

Peptide dynamics can be learned from heteronuclear NOE measurements when the peptide is isotope-labeled (Fig. 1b). For unlabeled peptides, such measurements are inconvenient. Current practice is to deduce dynamic information from an ensemble of NMR structures based on structural precision. However, there is no guarantee for the accuracy of such deduction because a lack of structural precision can be due to the lack of NMR restraints, due to protein motions, or due to both [1,6]. In the case of LL-37, a correlation between poor structural precision at the C-terminus and negative ^{15}N NOE values verified ps–ns time scale motions in that region. In the absence of isotope labeling, it may not be trivial to substantiate peptide motions based on structures. In Fig. 1, we illustrated a correlation between ^{15}N NOE and $^{13}C\alpha$ secondary shifts of LL-37. A correlation of protein motions on the fast (ns–ps) and slow (ms–s) time scales with $^{13}C\alpha$ secondary shifts was also observed for α-synuclein bound to SDS micelles [40]. These observations suggest that the $^{13}C\alpha$ secondary shifts may be harnessed as a probe for peptide dynamics, especially when isotope-labeled peptides are not available. Thus, aurein 1.2 is completely rigid upon binding to micelles (Fig. 3d), consistent with the well-defined all-helical structure (Fig. 4b). Using the same criteria, only residue V32 of GF-17 and R29 of KR-12 are likely to be mobile (Fig. 3).

The location of membrane peptides on micelles can be probed by different techniques. Spin labels can be incorporated into micelles followed by the examination of intensity changes of peptide peaks [6]. A more quantitative analysis can also be conducted to gauge the depth of the peptide penetration in micelles [41]. It is also possible to obtain such information without introducing additional probe molecules into NMR samples. For example, we previously used peptide–D8PG intermolecular NOE patterns to determine the location of the peptide on the micelles [22]. Furthermore, intermolecular NOE contacts were applied to determination of the membrane location of transmembrane β-barrel and helical proteins as well [42–44]. The wave pattern of the $^{1}H–^{13}C\alpha$ cross peaks in natural abundance HSQC spectra (dubbed HSQC waves) offers additional insight into peptide–micelle interactions. Several factors influence the wave patterns observed in the plots (Fig. 5). During polarization transfer from ^{1}H to ^{13}C and back to ^{1}H for detection, we know that both J coupling ($^{1}J_{CA\_HA}$) and transverse relaxation time (T_2) are in play. A survey of the one-bond $^{1}H–^{13}C\alpha$ coupling constants deposited in the Biological Magnetic Resonance Bank (http://www.bmrb.edu) [45] shows that hydrophobic residues do not preferentially display smaller coupling constants than

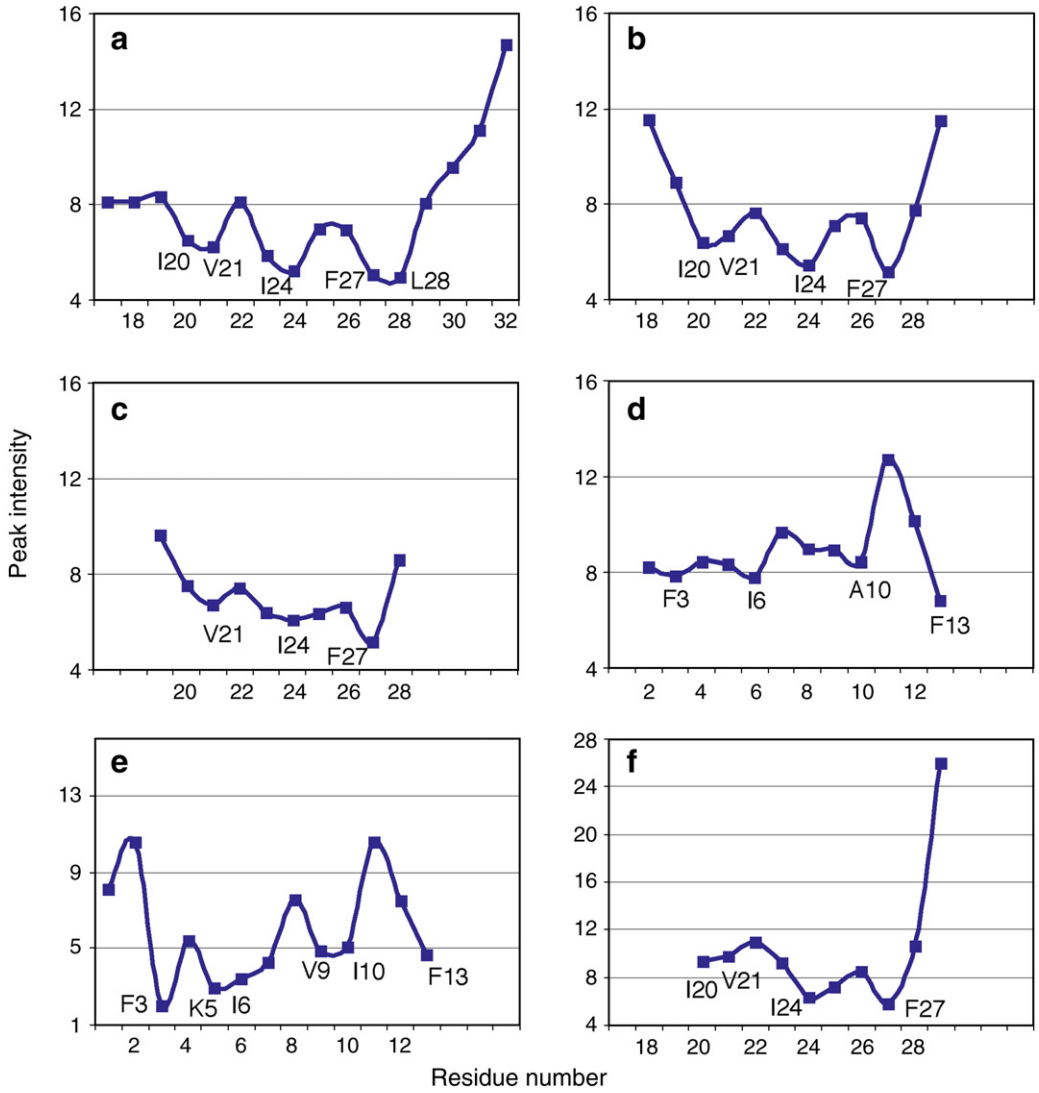

Fig. 5. HSQC waves of GF-17 (a), KR-12 (b), RI-10, aurein 1.2 (d), LL-37-derived aurein 1.2 analog (LLAA) (e) in complex with SDS micelles, and KR-12 in DPC micelles (f). The actual $^{1}H–^{13}C$ cross peak intensities as measured by NMRDraw [32] are the readings in the figures multiplied by 10,000. The pH, temperature, and peptide/detergent molar ratios for data in panels a–d are provided in Fig. 2. For LLAA, the NMR data were collected in SDS micelles at a peptide/SDS molar ratio of 1:40, pH 4.4, and 25 °C; for KR-12, the data were collected in DPC micelles at a peptide/DPC molar ratio of 1:60, pH 5.8, and 25 °C. The peak intensity of R19 of KR-12 in DPC close to water was not included here because it appeared to be less intense than I20 or V21 due to the effect of water suppression pulses.

hydrophilic residues. For example, the $^{1}J_{CA\_HA}$ coupling constant for asparagines ranges from 135.04 to 145.15 Hz, while the same coupling constant for valines also varies from 137.76 to 146.21 Hz. It appears that the polarization transfer between ^{1}H and $^{13}C\alpha$ is of similar efficiency for hydrophilic and hydrophobic residues. Thus, the location of hydrophobic residues in the troughs of the HSQC waves (Fig. 5) may be primarily due to the differential effect of T_2, which is directly related to line width or peak height of each residue. Specifically, fast exchange between the free and micelle-bound forms may be the dominating factor. This explanation would be in line with the known peak shifting and broadening of interfacial residues of proteins involved in protein–protein interactions, also due to fast exchange between the free and bound states [46]. In the case of ligand binding to the grooves on the protein surface, chemical shift mapping (based on chemical shift differences between the free and bound forms) is routinely applied in mapping binding residues on the protein surface [47]. For micelle-bound peptides with a global conformational change from the free to the bound states, this practice is complicated and the information is masked by substantial chemical shift changes in all micelle-bound residues. As an alternative explanation, which is more likely, the subtle peak intensity differences (Fig. 5) might be related to the degree of motion, leading to higher intensities for exposed residues and lower intensities for micelle-buried residues. Therefore, the $^{1}H–^{13}C$ HSQC waves observed here (Fig. 5) present a useful approach for identifying key membrane-binding residues of micelle-bound peptides by NMR. In particular, the consistent identification of phenylalanines as one of the key membrane anchors in all the cases concurs with intermolecular NOE observations that prove the insertion of the aromatic rings into lipid head group/acyl chain regions of micelles [1,6,39]. Moreover, the unique location of arginine side chain H^{N} signals in D8PG micelles enabled the detection of Arg–PG interactions by solution NMR [19,22,23]. In combination, these results depict a picture for membrane peptides that penetrate into the micelle head group region via hydrophobic anchoring residues and cationic side chains. The membrane surface location of human LL-37 deduced from solution NMR methods in micelle models [7,23] agrees with the measurements by solid-state NMR in lipid bilayers [12,55]. Clearly, results from solution NMR and solid-state NMR are complementary to each other [2,6]. While solution NMR is capable of elucidating entire 3D structures of AMPs in complex with micelles at the atomic resolution [5,19,27,53,64,65]; solid-state NMR can provide orientation and oligomerization information of AMPs in lipid bilayers [66–71].

It is worthwhile to point out that the wave concept has been applied to other NMR observables. Earlier, the periodicity of backbone amide proton chemical shifts of amphipathic peptides was observed. High amide chemical shift periodicity is treated as evidence for curved helices [48]. To illustrate this, we show that the amide proton plot of LL-37 in complex with SDS micelles (Fig. 1d) possesses a high degree of periodicity, indicating a curved helix. This is indeed the case in the calculated structure of LL-37 displayed in Fig. 1a. It is proposed that most of the residues with downfield shifts (F6, G14, F17, I20, K25, and L28 in Fig. 1d) form short (strong) hydrogen bonds [48]. Waves have also been observed in the paramagnetic NMR studies of micelle-bound peptides [41,49]. Temperature coefficient waves (plots of temperature coefficients of backbone amide protons versus polypeptide residue number) were illustrated to be useful in identifying exposed β-strands in β-sheet proteins, providing spatial restraints for chemical shift-based protein fold establishment [50]. This was attributed to the difference in hydrogen bonding patterns of amide protons in exposed and buried β-strands. Dipolar waves are particularly useful for mapping the structure and orientation of helices in membrane proteins [51]. The HSQC waves observed here shed novel insight into peptide–micelle interactions by mapping essential membrane-anchoring residues. For antimicrobial peptides, HSQC waves could guide site-directed mutagenesis to improve peptide therapeutic index by reducing peptide hydrophobicity based on both database findings and structure–activity relationship (SAR) studies [9,35]. The various waves discussed above may be unified under one umbrella and referred to as NMR waves that provide unique insight into the regular structure of polypeptides from different angles.

In conclusion, this study, along with our previous work [20], illustrates the applications of natural abundance HSQC spectra of short membrane-associated peptides without isotope labeling. Firstly, ^{15}N and ^{13}C chemical shifts can be utilized to substantiate ^{1}H assignments. They can also be used to generate dihedral angles for refinement of NOE-derived structures [6]. Secondly, the $^{13}C\alpha$ secondary shifts can be used to identify the structured regions and to judge whether some residues are mobile. Thirdly, HSQC waves may be exploited qualitatively to identify key residues for micelle binding. To obtain a reliable HSQC wave, NMR spectra should have sufficient signal to noise ratios, the peaks be correctly phased and well resolved, and the peak intensities should not be clearly reduced by the water suppression pulses. In this study, we have substantiated the importance of the identified key hydrophobic residues in KR-12 by single-residue mutation as well as intermolecular Phe-lipid NOE observations. With more and more examples, the generality of HSQC waves in identifying key membrane-anchoring residues of other membrane peptides will be tested. Considering the large number (>1400 entries) of short AMPs collected in APD2 and their therapeutic potential, natural abundance heteronuclear NMR should improve our knowledge on peptide–membrane interactions and peptide design.

Acknowledgements

The access to the NMR Core Facility of UNMC is appreciated. This NMR facility is supported by both the CORE Grant from NCI-NIH and the State of Nebraska through Nebraska Research Initiative. We thank Frank Delaglio and Dan Garrett (NIH) for providing updated NMR software and for useful discussion, Edward Ezell (UNMC) for maintaining the NMR hardware. Finally, we thank Eldon Ulrich (John Markley's lab) for providing a table of spin coupling constants.

References

[1] G. Wang, NMR of membrane-associated peptides and proteins, Curr. Protein Pept. Sci. 9 (2008) 50–69.
[2] S.J. Opella, F.M. Marassi, Structure determination of membrane proteins by NMR spectroscopy, Chem. Rev. 104 (2004) 3587–3606.
[3] S.H. Park, S. Prytulla, A.A. De Angelis, J.M. Brown, H. Kiefer, S.J. Opella, High-resolution NMR spectroscopy of a GPCR in aligned bicelles, J. Am. Chem. Soc. 128 (2006) 7402–7403.
[4] C. Tian, R.M. Breyer, H.J. Kim, M.D. Karra, D.B. Friedman, A. Karpay, C.R. Sanders, Solution NMR spectroscopy of the human vasopressin V2 receptor, a G protein-coupled receptor, J. Am. Chem. Soc. 127 (2005) 8010–8011.
[5] E.F. Haney, H.N. Hunter, K. Matsuzaki, H.J. Vogel, Solution NMR Studies of Amphibian Antimicrobial Peptides: Linking Structure to Function? Biochim. Biophys. Acta 1788 (2009) 1639–1655.
[6] G. Wang, Structural Biology of antimicrobial peptides by NMR spectroscopy, Curr. Org. Chem. 10 (2006) 569–581.
[7] F. Porcelli, R. Verardi, L. Shi, K.A. Henzler-Wildman, A. Ramamoorthy, G. Veglia, NMR structure of the cathelicidin-derived human antimicrobial peptide LL-37 in dodecylphosphocholine micelles, Biochemistry 47 (2008) 5565–5572.
[8] J.T. Cheng, J.D. Hale, M. Elliot, R.E. Hancock, S.K. Straus, Effect of membrane composition on antimicrobial peptides aurein 2.2 and 2.3 from Australian southern bell frogs, Biophys. J. 96 (2009) 552–565.
[9] Z. Wang, G. Wang, APD: the antimicrobial peptide database, Nucleic Acids Res. 32 (2004) D590–D592.
[10] G. Wang, X. Li, Z. Wang, APD2: the updated antimicrobial peptide database and its application in peptide design, Nucleic Acids Res. 37 (2009) D933–D937.
[11] B. Bechinger, M. Zasloff, S.J. Opella, Structure and dynamics of the antibiotic peptide PGLa in membranes by solution and solid-state nuclear magnetic resonance spectroscopy, Biophys. J. 74 (1998) 981–987.
[12] K.A. Henzler Wildman, D.K. Lee, A. Ramamoorthy, Mechanism of lipid bilayer disruption by the human antimicrobial peptide, LL-37, Biochemistry 42 (2003) 6545–6558.
[13] S. Yamaguchi, M. Hong, Determination of membrane Peptide orientation by 1H-detected 2H NMR spectroscopy, J. Magn. Reson. 155 (2002) 244–250.
[14] M.P. Boland, F. Separovic, Membrane interactions of antimicrobial peptides from Australian tree frogs, Biochim. Biophys. Acta 1758 (2006) 1178–1183.
[15] R.F. Epand, B.P. Mowery, S.E. Lee, S.S. Stahl, R.I. Lehrer, S.H. Gellman, R.M. Epand, Dual mechanism of bacterial lethality for a cationic sequence-random copolymer that mimics host-defense antimicrobial peptides, J. Mol. Biol. 379 (2008) 38–50.
[16] G. Wang, P.A. Keifer, A. Peterkofsky, Solution structure of the N-terminal amphitropic domain of *Escherichia coli* glucose-specific enzyme IIA in membrane-mimetic micelles, Protein Sci. 12 (2003) 1087–1096.
[17] G. Wang, P.A. Keifer, A. Peterkofsky, Short-chain diacyl phosphatidylglycerols: which one to choose for the NMR structural determination of a membrane-associated peptide from *Escherichia coli*? Spectroscopy 18 (2004) 257–264.
[18] P.A. Keifer, A. Peterkofsky, G. Wang, Effects of detergent alkyl chain length and chemical structure on the properties of a micelle-bound bacterial membrane targeting peptide, Anal. Biochem. 331 (2004) 33–39.
[19] G. Wang, NMR studies of a model antimicrobial peptide in the micelles of SDS, dodecylphosphocholine, or dioctanoylphosphatidylglycerol, Open Magn. Reson. J. 1 (2008) 9–15.
[20] G. Wang, Y. Li, X. Li, Correlation of three-dimensional structures with the antibacterial activity of a group of peptides designed based on a nontoxic bacterial membrane anchor, J. Biol. Chem. 280 (2005) 5803–5811.
[21] X. Li, Y. Li, A. Peterkofsky, G. Wang, NMR studies of aurein 1.2 analogs, Biochim. Biophys. Acta 1758 (2006) 1203–1214.
[22] G. Wang, Determination of solution structure and lipid micelle location of an engineered membrane peptide by using one NMR experiment and one sample, Biochim. Biophys. Acta 1768 (2007) 3271–3281.
[23] G. Wang, Structures of human host defense cathelicidin LL-37 and its smallest antimicrobial peptide KR-12 in lipid micelles, J. Biol. Chem. 283 (2008) 32637–32643.
[24] O. Cirioni, A. Giacometti, R. Ghiselli, C. Bergnach, F. Orlando, C. Silvestri, F. Mocchegiani, A. Licci, B. Skerlavaj, M. Rocchi, V. Saba, M. Zanetti, G. Scalise, LL-37 protects rats against lethal sepsis caused by gram-negative bacteria, Antimicrob. Agents Chemother. 50 (2006) 1672–1679.
[25] K. Pütsep, G. Carlsson, H.G. Boman, M. Andersson, Deficiency of antibacterial peptides in patients with morbus Kostmann: an observation study, Lancet 360 (2002) 1144–1149.
[26] V. Nizet, T. Ohtake, X. Lauth, J. Trowbridge, J. Rudisill, R.A. Dorschner, V. Pestonjamasp, J. Piraino, K. Huttner, R.L. Gallo, Innate antimicrobial peptide protects the skin from invasive bacterial infection, Nature 414 (2001) 454–457.
[27] T. Rozek, K.L. Wegener, J.H. Bowie, I.N. Olver, J.A. Caver, J.C. Wallace, M.J. Tyler, The antibiotic and anticancer active aurein peptides from the Australian Bell Frogs *Litoria aurea* and *Litoria raniformis* the solution structure of aurein 1.2, Eur. J. Biochem. 267 (2000) 5330–5341.
[28] J. Jeener, B.H. Meier, P. Bachmann, R.R. Ernst, Investigation of exchange processes by two-dimensional NMR spectroscopy, J. Chem. Phys. 71 (1979) 4546–4553.
[29] A. Bax, D.G. Davis, MLEV-17 based two-dimensional homonuclear magnetization transfer spectroscopy, J. Magn. Reson. 65 (1985) 355–360.
[30] M. Piotto, V. Saudek, V. Sklenar, Gradient-tailored excitation for single-quantum NMR spectroscopy of aqueous solutions, J. Biomol. NMR 2 (1992) 661–665.
[31] L.E. Kay, P.A. Keifer, T. Saarinen, Pure absorption gradient enhanced heteronuclear single quantum correlation spectroscopy with improved sensitivity, J. Am. Chem. Soc. 114 (1992) 10663–10665.
[32] F. Delaglio, S. Grzesiek, G.W. Vuister, G. Zhu, J. Pfeifer, A. Bax, NMRPipe: a multidimensional spectral processing system based on UNIX pipes, J. Biomol. NMR 6 (1995) 277–293.
[33] D.S. Garrett, R. Powers, A.M. Gronenborn, G.M. Clore, A common sense approach to peak picking two-, three- and four-dimensional spectra using automatic computer analysis of contour diagrams, J. Magn. Reson. 95 (1991) 214–220.

[34] G. Cornilescu, F. Delaglio, A. Bax, Protein backbone angle restraints from searching a database for chemical shift and sequence homology, J. Biomol. NMR 13 (1999) 289–302.
[35] X. Li, Y. Li, H. Han, D.W. Miller, G. Wang, Solution structures of human LL-37 fragments and NMR-based identification of a minimal membrane-targeting antimicrobial and anticancer region, J. Am. Chem. Soc. 128 (2006) 5776–5785.
[36] D.S. Wishart, B.D. Sykes, The ^{13}C chemical-shift index: a simple method for the identification of protein secondary structure using ^{13}C chemical-shift data, J. Biomol. NMR 4 (1994) 171–180.
[37] G. Wang, K.M. Watson, R.W. Buckheit Jr, Anti-human Immunodeficiency virus type 1 activities of antimicrobial peptides derived from human and bovine cathelicidins, Antimicrob. Agents Chemother. 9 (2008) 3438–3440.
[38] K. Wüthrich, NMR of Proteins and Nucleic Acids, Wiley, New York, 1986.
[39] G. Wang, Tool developments for structure–function studies of host defense peptides, Protein Pept. Lett. 14 (2007) 57–69.
[40] T.S. Ulmer, A. Bax, N.B. Cole, R.L. Nussbaum, Structure and dynamics of micelle-bound human -synuclein, J. Biol. Chem. 280 (2005) 9595–9603.
[41] K. Zangger, M. Respondek, C. Göbl, W. Hohlweg, K. Rasmussen, G. Grampp, T. Madl, Positioning of micelle-bound peptides by paramagnetic relaxation enhancements, J. Phys. Chem. B. 113 (2009) 4400–4406.
[42] K.J. Glover, J.A. Whiles, R.R. Vold, G. Melacini, Position of residues in transmembrane peptides with respect to the lipid bilayer: a combined lipid Noes and water chemical exchange approach in phospholipid bicelles, J. Biomol. NMR 22 (2002) 57–64.
[43] C. Fernández, C. Hilty, G. Wider, K. Wüthrich, Lipid–protein interactions in DHPC micelles containing the integral membrane protein OmpX investigated by NMR spectroscopy, Proc. Natl. Acad. Sci. U. S. A. 99 (2002) 13533–13537.
[44] J.H. Chill, J.M. Louis, C. Miller, A. Bax, NMR study of the tetrameric KcsA potassium channel in detergent micelles, Protein Sci. 15 (2006) 684–698.
[45] J.L. Markley, E.L. Ulrich, H.M. Berman, K. Henrick, H. Nakamura, H. Akutsu, BioMagResBank (BMRB) as a partner in the Worldwide Protein Data Bank (wwPDB): new policies affecting biomolecular NMR depositions, J. Biomol. NMR 40 (2008) 153–155.
[46] G. Wang, A. Peterkofsky, P.A. Keifer, X. Li, NMR characterization of the *Escherichia coli* nitrogen regulatory protein IIA^{Ntr} in solution and interaction with its partner protein, NPr. Protein Sci. 14 (2005) 1082–1090.
[47] G. Wang, M. Sondej, D.S. Garrett, A. Peterkofsky, G.M. Clore, A common interface on histidine-containing phosphocarrier protein for interactions with its partner proteins, J. Biol. Chem. 275 (2000) 16401–16403.
[48] N.E. Zhou, B.Y. Zhu, B.D. Sykes, R.S. Hodges, Relationship between amide proton chemical shifts and hydrogen bonding in amphipathic helices, J. Am. Chem. Soc. 114 (1992) 4320–4326.
[49] R. Bussell Jr., T.F. Ramlall, D. Eliezer, Helix periodicity, topology, and dynamics of membrane-associated a-synuclein, Protein Sci. 14 (2005) 862–872.
[50] X. Li, A. Peterkofsky, G. Wang, Solution structure of NPr, a bacterial signal-transducing protein that controls the phosphorylation state of the potassium transporter-regulating protein IIA^{Ntr}, Amino Acids 35 (2008) 531–539.
[51] M.F. Mesleh, G. Veglia, T.M. DeSilva, F.M. Marassi, S.J. Opella, Dipolar waves as NMR maps of protein structure, J. Am. Chem. Soc. 124 (2002) 4206–4207.
[52] R. Koradi, M. Billeter, K. Wüthrich, MOLMOL: a program for display and analysis of macromolecular structures, J. Mol. Graph. 14 (1996) 51–55.
[53] R.P. Nanga, J.R. Brender, J. Xu, G. Veglia, A. Ramamoorthy, Structures of rat and human islet amyloid polypeptide IAPP(1–19) in micelles by NMR spectroscopy, Biochemistry 47 (2008) 12689–12697.
[54] R.P. Nanga, J.R. Brender, J. Xu, K. Hartman, V. Subramanian, A. Ramamoorthy, Three-Dimensional Structure and Orientation of Rat Islet Amyloid Polypeptide Protein in a Membrane Environment by Solution NMR Spectroscopy, J. Am. Chem. Soc. 131 (2009) 8252–8261.
[55] K.A. Henzler-Wildman, G.V. Martinez, M.F. Brown, A. Ramamoorthy, Perturbation of the hydrophobic core of lipid bilayers by the human antimicrobial peptide LL-37, Biochemistry 43 (2004) 8459–8469.
[56] U.H. Dürr, U.S. Sudheendra, A. Ramamoorthy, LL-37, the only human member of the cathelicidin family of antimicrobial peptides, Biochim. Biophys. Acta 1758 (2006) 1408–1425.
[57] Y. Yang, G. Zheng, G. Li, X. Zhang, Z. Cao, Q. Rao, K. Wu, Expression of bioactive recombinant GSLL-39, a variant of human antimicrobial peptide LL-37, in Escherichia coli, Protein Expr. Purif. 37 (2004) 229–235.
[58] Y. Li, X. Li, G. Wang, Cloning, expression, isotope labeling, and purification of human antimicrobial peptide LL-37 in Escherichia coli for NMR studies, Protein Expr. Purif. 47 (2006) 498–505.
[59] J.Y. Moon, K.A. Henzler-Wildman, A. Ramamoorthy, Expression and purification of a recombinant LL-37 from Escherichia coli, Biochim. Biophys. Acta 1758 (2006) 1351–1358.
[60] A. Nijnik, R.E. Hancock, The roles of cathelicidin LL-37 in immune defences and novel clinical applications, Curr. Opin. Hematol. 16 (2009) 41–47.
[61] J. Johansson, G.H. Gudmundsson, M.E. Rottenberg, K.D. Berndt, B. Agerberth, Conformation-dependent antibacterial activity of the naturally occurring human peptide LL-37, J. Biol. Chem. 273 (1998) 3718–3724.
[62] Z. Oren, J.C. Lerman, G.H. Gudmundsson, B. Agerberth, Y. Shai, Structure and organization of the human antimicrobial peptide LL-37 in phospholipid membranes: relevance to the molecular basis for its non-cell-selective activity, Biochem. J. 341 (1999) 501–513.
[63] M. Zanetti, The role of cathelicidins in the innate host defenses of mammals, Curr. Issues Mol. Biol. 7 (2005) 179–196.
[64] A. Ramamoorthy, S. Thennarasu, D.K. Lee, A. Tan, L. Maloy, Solid-state NMR investigation of the membrane-disrupting mechanism of antimicrobial peptides MSI-78 and MSI-594 derived from magainin 2 and melittin, Biophys. J. 91 (2006) 206–216.
[65] S. Thennarasu, D.K. Lee, A. Tan, U. Prasad Kari, A. Ramamoorthy, Antimicrobial activity and membrane selective interactions of a synthetic lipopeptide MSI-843, Biochim. Biophys. Acta 1711 (2005) 49–58.
[66] K.J. Hallock, D.K. Lee, J. Omnaas, H.I. Mosberg, A. Ramamoorthy, Membrane composition determines pardaxin's mechanism of lipid bilayer disruption, Biophys. J. 83 (2002) 1004–1013.
[67] A. Ramamoorthy, D.K. Lee, J.S. Santos, K.A. Henzler-Wildman, Nitrogen-14 solid-state NMR spectroscopy of aligned phospholipid bilayers to probe peptide-lipid interaction and oligomerization of membrane associated peptides, J. Am. Chem. Soc. 130 (2008) 11023–11029.
[68] S.K. Kandasamy, D.K. Lee, R.P. Nanga, J. Xu, J.S. Santos, R.G. Larson, A. Ramamoorthy, Solid-state NMR and molecular dynamics simulations reveal the oligomeric ion-channels of TM2-GABA(A) stabilized by intermolecular hydrogen bonding, Biochim. Biophys. Acta 1788 (2009) 686–695.
[69] A. Ramamoorthy, S.K. Kandasamy, D.K. Lee, S. Kidambi, R.G. Larson, Structure, topology, and tilt of cell-signaling peptides containing nuclear localization sequences in membrane bilayers determined by solid-state NMR and molecular dynamics simulation studies, Biochemistry 46 (2007) 965–975.
[70] M. Hong, Oligomeric structure, dynamics, and orientation of membrane proteins from solid-state NMR, Structure 14 (2006) 1731–1740.
[71] A. Ramamoothy, N.M.R. Beyond, spectra of antimicrobial peptides: dynamical images at atomic resolution and functional insights, Solid State Nucl. Magn. Reson. 35 (2009) 201–207.
[72] R.F. Epand, G. Wang, B. Berno, R.M. Epand, Lipid clustering explains the antimicrobial activity of fragments of the human cathelicidin LL-37, Antimicrob. Agents Chemother. 53 (2009) 3705–3714.